Granular Matter (2013) 15:367–376
DOI 10.1007/s10035-013-0397-9

ORIGINAL PAPER

Effect of the confinement on the properties of ultrasonic vibrated granular gases

J. Badreddine · M. Micoulaut · E. Rouhaud · S. Remy · D. Retraint · M. François

Received: 9 May 2012 / Accepted: 1 February 2013 / Published online: 16 March 2013

Abstract The properties of a ultrasonic vibrated granular gas are investigated by using an event-driven Molecular Dynamics simulation of inelastic hard spheres that are fluidized by a vibrating bottom wall (sonotrode) in boxes with different geometries showing either no or an increased confinement. It appears that geometry controls dramatically not only the distribution of wall impacts and their velocity and impact angles, but also more fundamental properties of the granular gas such as temperature and density. For geometries displaying an acute angle (prism), stacking is found, which induces a strong temperature and density gradient. The underlying origin of such phenomena for the granular gas arises from the spatial limitation, confinement, combined with the inelastic collisions induced by closely located side walls. It underscores the possibility that kinetic and thermodynamic properties of granular gases can be changed by simple geometries inducing spatial limitation.

Keywords Application of granular gases · Event-driven simulation · Geometry

Electronic supplementary material The online version of this article (doi:10.1007/s10035-013-0397-9) contains supplementary material, which is available to authorized users.

J. Badreddine · E. Rouhaud · S. Remy · D. Retraint · M. François
Laboratoire des Systémes Mécaniques et d'Ingénierie Simultanée (LASMIS), 12 rue Marie Curie, 10010 Troyes, France

M. Micoulaut (✉)
Laboratoire de Physique Théorique de la Matiére Condensée, Université Pierre et Marie Curie, 4 Place Jussieu, 75252 Paris Cedex 05, France
e-mail: mmi@lptl.jussieu.fr

1 Introduction

Granular materials are important systems in a large number of industrial processes and geophysical phenomena [1]. However, despite many efforts both on the experimental and theoretical side, no fundamental description is currently available to describe their physical properties. Nevertheless, it has been shown that many of the usual features derived from the statistical mechanics description of molecular systems can be recovered in granular ones [2,3]. This is especially true for dilute media where the concepts and methods of kinetic gas theory apply rather well to granular gases [4]. For dense media the off-equilibrium properties are even enhanced so that many open questions remain [5]. Furthermore, the properties of a collection of grains is very complex and can display a variety of surprising collective behaviors such as ageing [6], convection [7], pattern formation [8] and size separation [9], depending on the system density and/or the degree of inleasticity during the collisions.

In the field of industrial applications, focus has been mostly made on the properties of the granular material itself [10], leaving apart the possibility to use a granular medium as an interfacing agent for another material of industrial interest. One well-known example of such alternative possibilities is found in tribology [11]: wear is produced on a materials surface by e.g. abrasion or friction, the latter being produced by a collection of grains. In mechanical engineering, it has been also shown that granular gases could be identified with shot in peening processes which are used in automotive and aerospatial industry [12,13]. Here, a high velocity stream of particles of millimetric size is projected at surface of the material, producing at and below its surface compressive residual stresses, which increase fatigue life. A recent promising technique in this field, ultrasonic shot peening, has been proposed [14] and consists in the projection of the spheres by using an ultrasonic (20 kHz) vibrating bottom wall.

Obviously, there is a striking analogy between ultrasonic shot peening and a vibrated granular gas.

Little is known about the properties of the shot. In the peening process, a piezoelectric generator produces the vibration of a bottom wall (a sonotrode); this projects upon contact the spheres in a chamber closed by a top cover, the latter being the sample whose surface is planed to be hardened. There are obvious control parameters such as the number of spheres, the amplitude and frequency of the sonotrode, etc. which have a direct impact on the overall properties of the shot. However, there is of course no direct relationship between such parameters and the relevant properties of the impacting spheres (velcocity, angle, frequency, position, etc.), although it is necessary to optimize the residual stress field appearing with surface hardening. Models derived for granular gases may therefore be particularly welcome, and can e.g. allow to predict the coverage rate, a very important quantity in surface treatment [15].

In this article, we study the effect of the chamber geometry on the properties of a vibrated granular gas in the context of ultra sound shot peening (see supplementary material). To be consistent, we work at ultrasonic frequencies (20 kHz), and with amplitudes usually found in such processes. Three different geometries with the same gas density are considered: a cylinder, a box with a square base and a trapezoidal prism with changing top angle (Fig. 1). There is an underlying reason to perform such kind of studies. In standard ultrasonic shot peening processes, it is frequent to have the top surface tilted with respect to the sonotrode. A prism is therefore the simplest geometry that can be considered in a simulation box if one attempts to analyze the behavior of a vibrated shot when top and bottom walls are not parallel.

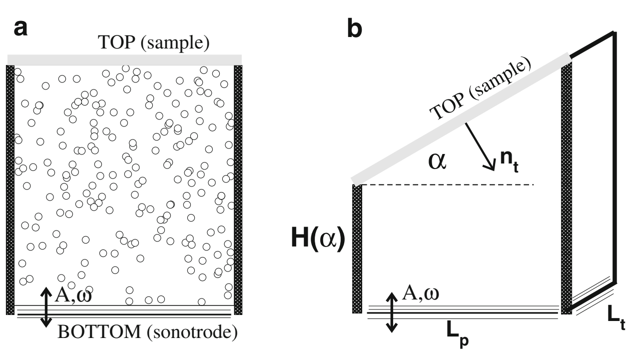

Fig. 1 Shot peening setup and geometries used in this study: **a** Cylinder or box with square base. **b** Trapezoidal prism with changing angle α. The *bottom* wall is the sonotrode, characterized by its amplitude A and vibration frequency ω, and the *top* wall (in *grey*) is the peened sample. In the chamber N spheres collide. L_p and L_t correspond to the longitudinal (x) and transverse (y) direction of the base, respectively

Our results show that the geometry strongly influences the properties of the granular gas such as impact velocity, impact angle and impact distribution but also the spatial distribution of thermodynamic quantities such as granular temperature or density. These changing properties are largely dominated by the inelastic collisions on the side walls, which produce adsorption, and lead to sphere stacking in some particular places where space is limited, inducing substantial density variations inside the box. In the present contribution, we show that velocity and angular impact distribution contain features that can be attributed to particular areas of the granular gas. Moreover, spatial limitation and stacking induce more surprising phenomena in the case of certain geometries [7]. We find an enhanced stacking close to the acute angle on top of the prism, which acts as a trap for the spheres, and changes substantially the global motion of the untrapped ones. As a result, the velocity field of the granular gas is much more complex than in simple geometries. Overall, these results highlight the crucial role played by the boundary in finite systems, and open the perspective to tune the properties of the granular gas simply by changing the shape of the chamber.

These results are obtained with a model of inelastic hard spheres, the collision rules and the details of the simulation being given in Sect. 2. Then, Sect. 3 describes the results. Section 4 provides an analysis of the results obtained in the previous section, and a discussion. We finally summarize and draw some conclusions.

2 Model details

The model (in 3D) that is considered here, is very close to an experimental setup used for ultrasonic shot peening [14], i.e. it contains $N = 200$ hard spheres of diameter $\sigma = 3$ mm representing the shot. The chosen number of spheres corresponds to what is usually fixed by experimental conditions in surface mechanical attrition treatments using shot peening [16]. The spheres are accelerated by a vibrating bottom wall of frequency 20 kHz and an amplitude A of 25 µm (see details below). The starting cylindrical geometry is also similar to what is used in such ultrasonic applications, i.e. it has a radius of R = 35 mm and a height of 40 mm leading to a gas density of $\eta = 1.3 \times 10^{-3}$ mm^{-3} and a volume $V_0 = 153.9 \times 10^3$ mm^3 corresponding to a solid fraction $\phi = 0.018$. In the forthcoming, when considering different chamber geometries, we will adapt the lengths in order to work at fixed density η and box volume V_0.

The system of spheres which are subject to a constant gravitational force, is found to be out of equilibrium as energy is lost through inelastic collisions. Energy is supplied with a vibrating bottom wall having a symmetric triangular profile characterized by an amplitude A and a period T given by the experimental setup. The use of such a profile allows to solve analytically the equation of motion before and after a bounce on the bottom wall, and thus the time of a collision between a particle and the bottom wall. An implicit equation (needing a more expensive numerical computation) would appear if an exact sinusoidal profile were to be considered. It should be noted that the choice of this triangular profile has no major impact on the results [13], because the amplitude of the harmonic n of the profile falls as odd n^{-2}. Furthermore, in the experimental setup, even though the electrical excitation of the bottom wall is sinusoidal, the velocity applied to the spheres at a bottom impact is certainly not purely sinusoidal because of the elastic deformation of the sonotrode. To the best of our knowledge, no experimental measurements on the elastic deformation of the sonotrode has been reported whereas such deformations are of course negligible at much lower frequency [7]. The present triangular profile can thus be considered as a realistic simplification to allow analytical computations. However, in order to check for consistency of the results, we have performed a single simulation with the same operating conditions (frequency, amplitude, shot density) using a parabolic expansion of a sinusoidal profile. Results show that the impact velocity and impact angle distribution remain nearly the same. We reserve the study of the effect of the vibrating profile for future work.

Initially, the spheres are placed randomly close to the sonotrode. An intermediate régime (t<0.5–1 s) sets in which depends on the initial conditions. For larger times, initial conditions do not alter the properties of the granular gas. One then has an non-equilibrium steady state over which statistical averages are accumulated.

The spheres collide inelastically and instantaneously with each other, with the side walls, with the top wall and with the bottom wall (sonotrode). The different collision rules are given by the following expressions involving velocity restitution coefficients:

Shot/side wall impact:

$$\mathbf{v}'_{i,n} = \mathbf{v}_{i,n} - (1 + c_N^w)(\mathbf{v}_{i,n}.\hat{\mathbf{n}}_w)\hat{\mathbf{n}}_w \tag{1}$$

Shot/sonotrode impact:

$$v'_{i,z} = v_{i,z} - (1 + c_N^b)(v_{i,z} - v_S) \tag{2}$$

Shot/top wall impact:

$$\mathbf{v}'_{\mathbf{i}}.\mathbf{n}_t = -c_N^t \mathbf{v}_{\mathbf{i}}.\mathbf{n}_t \tag{3}$$

Shot/shot impact:

$$\mathbf{v}'_{i,j} = \mathbf{v}_{i,j} \pm \frac{1 + c_N^s}{2}[(\mathbf{v}_j - \mathbf{v}_i).\hat{\mathbf{n}}]\hat{\mathbf{n}} \tag{4}$$

where the prime quantities denote the post-collisional quantities; $\mathbf{v}_{i,n}$ is the velocity component of the sphere i associated to the normal vector $\hat{\mathbf{n}}_w$ of the side-wall surface, and c_N^w is the normal coefficient of restitution for a collision between a sphere and the side walls of the chamber. v_S is the vertical velocity of the sonotrode ; $\mathbf{n}_t$ is the normal vector of the top wall, and c_N^t the normal coefficient of restitution for a collision between a sphere and the top wall. Note also that $\mathbf{n}_t$ corresponds to a vertical normal vector for the cylinder, the cube and the trapezoidal prism with $\alpha = 0°$. $v_{i,z}$ is the vertical component of the velocity of particle i ; finally, $\mathbf{v}'_{i,j}$ denote the velocities of i or j particle, $\hat{\mathbf{n}}$ is the unit center-to-center vector between the colliding pair i and j and c_N^s is the normal coefficient of restitution for a sphere-sphere collision. Between collisions, the spheres follow parabolic trajectories (free flight) due to the constant gravitational field, viscous damping with the air contained in the chamber being neglected. Obviously, a change in chamber geometry will affect Eqs. (1) and (3) while leaving Eqs. (2) and (4) unmodified.

The restitution coefficients c_N^i are taken as velocity dependent. For instance, it is well known from experiments that in the high velocity limit where plastification occurs, the restitution coefficient behaves as a power-law [17] of the form $v^{-1/4}$. In the low velocity range where deformations are supposed to be elastic and dissipation described by visco-elasticity [18,19], a slightly different power-law has been obtained [20], of the form: $(1-v^{1/5})$. We remind that the restitution coefficients depend also strongly on the sphere density, the sphere diameter [21], the thickness of the impacted surface [22], or even the impact angle [23]. However, beyond these more subtle dependences, a generic behaviour can be proposed, which is splitted into a low-velocity régime with low dissipation where c_i depends weakly on the impact velocity and can be considered as nearly constant, and a high velocity and more dissipative regime induced by plasticity (or even fracturing) where a power-law behaviour can be applied with confidence. In the forthcoming, we will use the following dependence for the normal restitution coefficient:

$$c_N^i(v) = \begin{cases} c_0^i, & v \leq v_0^i, \\ c_0^i \left(\frac{v}{v_0^i}\right)^{-1/4} & v \geq v_0^i \end{cases} \tag{5}$$

where v_0^i is a threshold velocity separating the visco-elastic from the plastic deformation régime, c_0^i is the low-velocity constant normal restitution coefficient with $i = b, t, w, s$, depending on the nature of the impacted surface (bottom, top, wall, spheres). It should be noted that the spheres never reach the elastic limit ($c_N^i = 1$) as $c_N^i(v) \rightarrow c_0^i$ when $v \rightarrow 0$. Parameters used in the following are given in Table 1. They have been chosen to reproduce experimental conditions and parameters have been fitted from sphere bounce experiments according to the nature of the impacted surface [12,24]. In principle, plastification of the materials at high impact velocity should harden the material so that collisions may have a different

Table 1 Parameters used for the velocity-dependent collision rules (5) of the inelastic spheres

Impacted material	i	c_0^i	v_0^i (cm/s)
Sonotrode (titanium)	b	0.91	1.2
Spheres (steel)	s	0.91	1.2
Sample (aluminium)	t	0.6	0.12
Side walls (alumnium)	w	0.6	0.12

rebound with increasing time. Such subtle details can not be taken into account in the present simulation but we have checked that the overall results do not depend crucially on the parameters involved in Eq. (5) as a change in c_0^i by ±50 % does not alter the conclusions of the study.

Recently, simulations of inelastic hard spheres [25] have been performed using Eq. (5). These have shown that an increased accuracy with experimental measurements and observation is obtained with a velocity-dependent normal restitution coefficient. Results have also shown that the unphysical clustering tendency of spheres was reduced with the use of velocity dependent restitution coefficients. Pressure effects as a function of the density of spheres could also be recovered by simulation for a dilute or dense vibrated granular medium.

In addition to Eq. (5), and in contrast with [25], we also use tangential restitution coefficient to account in an effective and simple way for transverse dissipation of energy. It becomes necessary if one wants to avoid unphysical side wall adsorbed ascendant spheres which appear from the bounce on the vibrating bottom wall and the inelastic collapse along the normal direction of the side-walls. In fact, if $c_T = 1$ and if $c_N^w(v)$ follows Eq. (5), there is a possibility that $\mathbf{v}'_{i,n}$ becomes small while the transverse velocity remains unchanged after impact. These effects are clearly not observed experimentally. The simplest way to account for the transverse dissipation is proposed by Brach [26]. Conservation of the angular momentum leads indeed to:

$$\frac{2}{5}m\left(\frac{\sigma}{2}\right)^2(\omega' - \omega) = m\frac{\sigma}{2}(v'_T - v_T) \tag{6}$$

where ω' and ω represent the rotational velocities after and before impact respectively, v'_T and v_T being the respective transverse impact velocities. If one assumes that there is no rotation ($\omega = 0$) and that there is rolling prior to departure of the sphere from the impacted surface, one has: $v'_T = (\sigma/2)\omega'$ which, in combination with Eq. (6) and the definition $v'_T = c_T v_T$, leads to $c_T = 5/7$ used in the following. Experiments on steel sphere bouncing [23] have shown that the constant value of 5/7 for c_T is verified for impact angles (under certain conditions) up to $\simeq 55°$.

The trajectories of the spheres are then tracked in an event-driven Molecular Dynamics simulation that detects the shortest time ellapsed between all possible collisions in the chamber and updates the trajectories accordingly. The collisions with their properties (velocity, angle, position, etc.) are recorded for analysis, and the number of total collisions for a simulation is set to about 10^5, corresponding to a total time of about 30 s.

With the number of spheres set to $N = 200$ and a gas density of $\eta = 1.3 \times 10^{-3}\text{mm}^{-3}$, the dimension of the different chambers have been taken as following to maintain the same volume V_0: a) a cylinder with 35 mm radius and 40 mm height ; b) a box of 62 mm height and a square base with 40 mm length ; and c) a trapezoidal prism with a rectangular base of size $L_p = 85$ mm in the longitudinal direction and $L_t = 36$ mm in the transverse direction, and a height $H(\alpha)$ (see Fig. 1b) given on the lower vertical side by:

$$H(\alpha) = \frac{V_0}{L_p L_t} - \frac{L_p}{2}\tan\alpha \tag{7}$$

We now study the properties of a granular gas confined in different geometries.

3 Results

Figure 2 shows the impacts for three different geometries at a fixed number of impacts (10^4) on the top wall. It should be noted that this does not correspond to the same simulation time. From the figure, it becomes clear that the impact distribution depends strongly on the chamber geometry. A heterogeneous distribution is found for the cylinder with an increased number of impacts on the border of the surface. This heterogeneity is found to be increased for the cube (Fig. 2b) with a large number of impacts found close to the edges of the cube, and less impacts at the center. The trapezoidal prism (Fig. 2c) displays a different pattern with an increased number of impacts close to the acute angle (here $90° - 40° = 50°$) whereas the edge defined by the obtuse angle ($90° + 40° = 130°$) has clearly a limited number of impacts. The motion of these spheres trapped in the vicinity of the side walls is ascendant due to the vibrating wall projecting spheres upwards. This effect of sphere-wall adsorption has been found to be one order of magnitude larger than the simple heterogeneity arising from boundary collisions close to the top wall [13]. It clearly shows that the inelastic sphere collisions with the side wall are relevant for understanding the heterogeneous shot peening which is manifested by an increased impact number on the border of the sample. Non-elastic collisions on the side walls originate the impact profile that is also experimentally observed.

The observed impact distribution can be quantified by following the impact frequency per unit surface (IFUS) as a function of the longitudinal coordinate L_p. Indeed, the

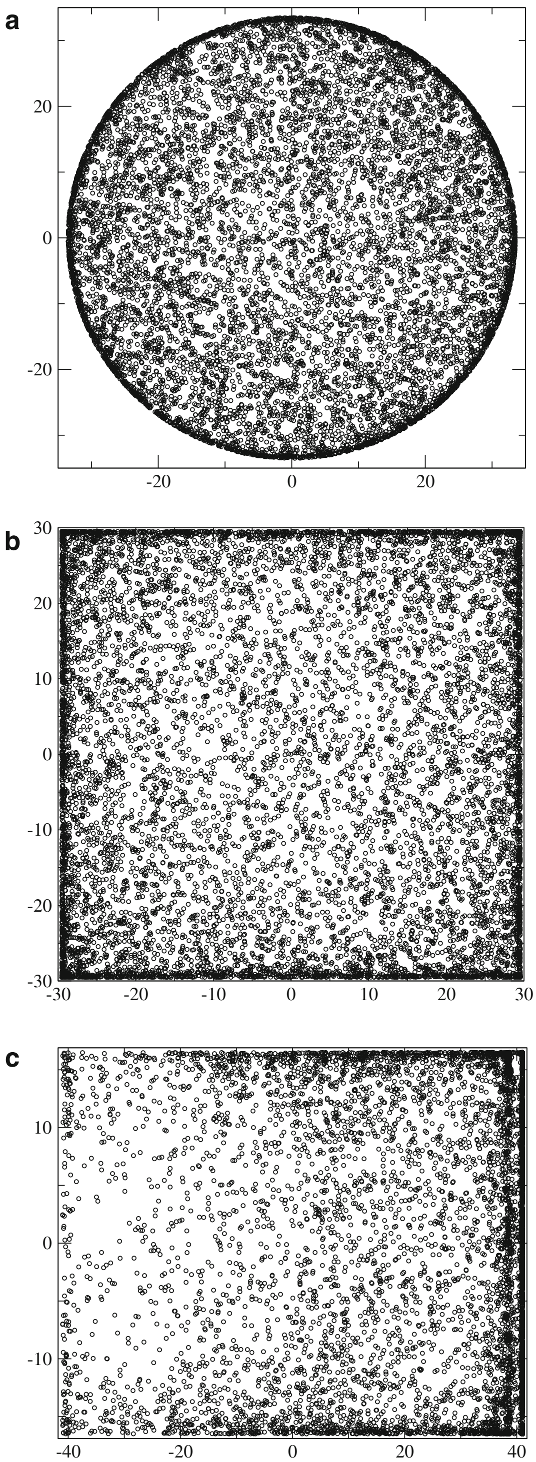

Fig. 2 Impacts (10^4) on the *top* wall for three different geometries. **a** Cylinder. **b** *Box* with *square* base. **c** Trapezoidal prism with $\alpha = 40°$

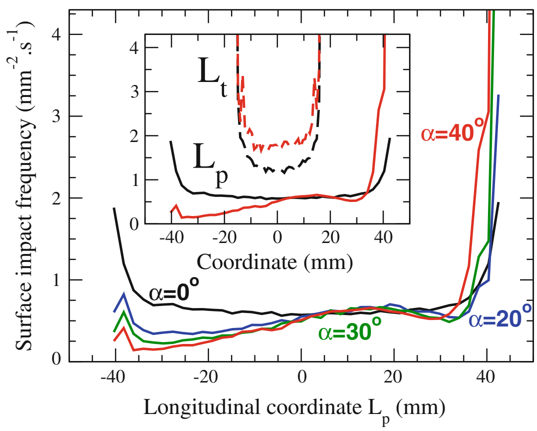

Fig. 3 (Color online) Surface impact frequency on the *top* wall for different chamber geometries (trapezoidal prism with for various angles α). The *insert* shows the same quantities for two selected angles ($\alpha = 0$, *black* and 40°, *red*) along the longitudinal coordinate L_p (*solid line*, same as b) and transverse coordinate L_t (*broken lines*)

number of impacts scales linearly with time which allows defining a frequency. Results are shown in Fig. 3. Here, one can notice the large heterogeneity found at the border of the chambers for all possible geometries which manifests by a large increase of the IFUS close to the border. The IFUS of the box with a square base and the cylinder are found to be similar in the center of the box.

Having in mind the crucial role played by the inelastic collisions on the side walls, we can analyze results for the trapezoidal prism displayed in Fig. 3. Although the shape of the box is different, results found for $\alpha = 0°$ are very close to those obtained for the box with a square base, i.e. a nearly constant IFUS at the center and a growth at the border of about twice the impact surface frequency of the center (Fig. 3). A similar behaviour is found for the transverse direction L_t of the box (Fig. 3, insert). When α becomes non-zero, the combination of spatial limitation created by the presence of an acute angle on the top of the prism box, and the tendency to adsorption due to inelastic side wall collisions, lead to an increased IFUS with increasing angle α. Indeed, with respect to the center of the chamber where the IFUS is found to be of about 0.5 (Fig. 3), the same quantity is multiplied by a factor ranging between 4 and 10 close to the side wall containing the acute angle. Of special interest is the maximum found for the IFUS close to a box length $L_p = 10$ mm for e.g. $\alpha = 40°$, also seen qualitatively from the impact distribution of Fig. 2c. The origin of this peak can be elucidated, as discussed below.

The nature of the impacts can be furthermore characterized by following the velocity $f_{impact}(v)$ and the impact angle $P(\theta)$ distributions as shown in Figs. 4 and 5. We first focus on the former (Fig. 4). For all geometries (Fig. 4), a peak at high velocity (typically 4.5 m/s) is found and corresponds typically to 4–5 % of the sphere impacts. In the prism geometry, this peak is found to shift to lower velocities when α is increased, i.e. from 4.5 m/s for $\alpha = 0°$ to 3.8 m/s for $\alpha = 40°$. We further analyze the origin of these features in the next section. A second peak is found at low velocity (0.2–0.3 m/s) which is also found to be nearly independent

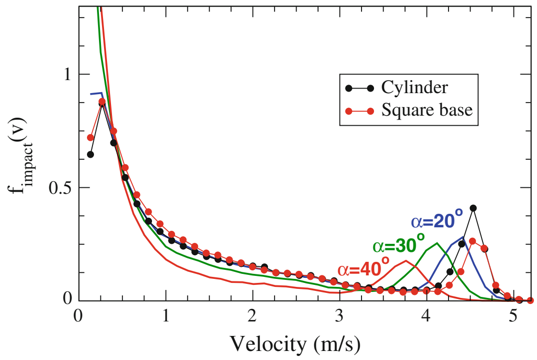

Fig. 4 (Color online) Normal impact velocity distribution $f_{impact}(v)$ for different chamber geometries : *Box* with *square* base and *cylinder* (*filled circles*), and trapezoidal prism with for various angles α (*unmarked solid lines*)

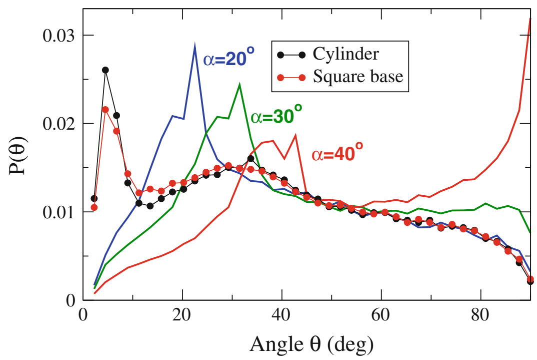

Fig. 5 (Color online) Impact angle distribution $P(\theta)$ for different chamber geometries: *Box* with a *square* base and *cylinder* (*filled circles*), and trapezoidal prism with various angles α (*unmarked solid lines*)

of the geometry (cylinder, box), provided that the angle α is not too high.

The impact angle distribution is displayed in Fig. 5. For such a dilute system ($\eta = 1.3 \times 10^{-3}\,\text{mm}^{-3}$) and when $\alpha = 0°$ (cylinder or square base), a prepeak is found at low angles, typically 10°, corresponding to quasi-vertically bouncing between the bottom and the top walls. When the granular gas density is increased (or N), this peak is found to disappear [13], i.e. it is a reminiscent feature of the case of infinite dilution. In the vicinity of the top wall, given the increased local density of the granular gas (see below), an increased number of sphere-sphere collisions is found which leads to oblique collisions on the top wall, resulting in the broad maximum found at 30° (Fig. 5 for the cylinder or the square base). No impacts with tangential incidence (i.e. 90°) are obtained.

New features appear when α becomes non-zero. First, we note that the peak resulting from the quasi-vertically bounce between bottom and top walls is shifted by the same angle as the change in geometry (or α), i.e. the contribution to the quasi-vertical bounce is now found at 40–42° when $\alpha = 40°$.

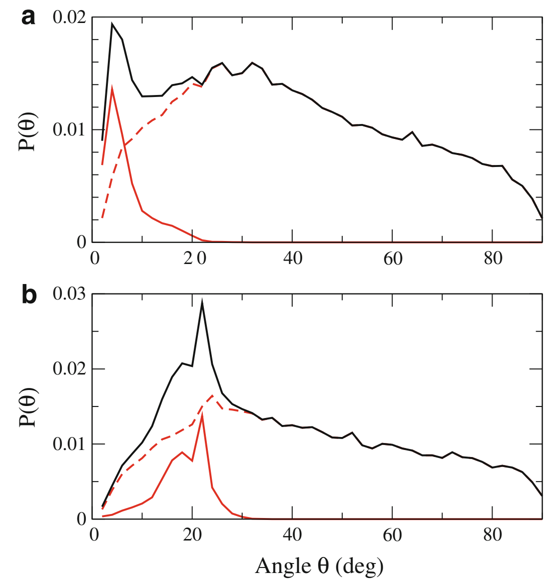

Fig. 6 (Color online) Impact angle distributions $P(\theta)$ in the prism box for $\alpha = 0$ (**a**) and $\alpha = 20°$ (**b**). Total distribution (*black solid line*, same as Fig. 5) and distributions with either $v < 4$ m/s (*red broken line*) or $v > 4$ m/s (*red solid line*)

This is a trivial effect as highlighted both from Fig. 1b and Eq. (3). On the other hand, a contribution at 90° builds up with increasing angle, and becomes dominant when α changes from 30 to 40°. We can thus conclude that tangential impacts are more and more present when the top angle of the prism becomes acute, and these will contribute substantially for $\alpha = 40°$.

4 Discussion

In the following, we want to focus on a certain number of features that have been described above, and which do not have a straightforward origin, for instance the maximum found in the IFUS close to the center of the top wall (Figs. 2b, 3) when α increases, the peak at high velocity in the velocity distribution (Fig. 4), and the increase of a contribution close to 90° in the impact angle distribution when α is increased (Fig. 5).

4.1 Velocity-angle correlations

Correlations between impact angles and impact velocities can be established. Those are represented in Fig. 6 for the trapezoidal prism with angle $\alpha = 0$ (top) or $\alpha = 20°$ (bottom). It appears that the main peak found in the impact angle distribution $P(\theta)$ of Fig. 5 is related to spheres with high normal impact velocities, i.e. those contributing to the high velocity peak at $\simeq 4.5$ m/s in the impact velocity distribution $f_{impact}(v)$ displayed in Fig. 4. In fact, by setting a limit at 4 m/s, i.e. somewhat lower than the high velocity peak of $f_{impact}(v)$, we find that the main peak in $P(\theta)$ arises entirely from such high velocity spheres. This correlation remains valid for the other investigated angles.

4.2 Velocity field

To gain additional insight, we compute the velocity field of the granular gas at different angles α in the prism geometry, averaged over the transverse coordinate L_t of the box. Results are shown in Fig. 7 for the angles $\alpha = 0°$, 20° and 40°.

For $\alpha = 0°$, we find the upwards accelerated trajectory with a small velocity gradient in the L_p direction, indicative of the sphere-wall adsorption effect resulting in lower velocities close to the box edges. This contrasts with results found for a cylinder geometry where a torroidal convection roll is obtained [7]. The latter is, again, mainly influenced by the side wall inelastic side collisions, with spheres being upwards accelerated by the sonotrode. Note that there is of course continuity (ρv = cst) in the system as downwards oriented moving spheres with low velocities mostly belong to dense regions located close to the top and side walls. On the other hand, high velocity spheres are accelerated upwards from the sonotrode in dilute regions of the box. These effects clearly appear when the motion of all spheres is tracked over a given simulation time (see the movie in supplementary material). This general feature is found to be robust and does not depend on e.g. the frequency and/or the degree of inelasticity of the collision rules as it has been found for at least two very different situations[7,13]. When α becomes non-zero, a new situation appears which is responsable for the observed features in Fig. 5 (growth of an impact angle of 90°) and Fig. 3 (local maximum of the IFUS). The increase of α makes the top angle of the prism more and more acute so that an increased number of spheres moving in the upper part of the box are influenced by this spatial limitation and can remain trapped in this part of the box. This effect is due to an increased number of sphere-sphere and sphere-wall inelastic collisions, leading to a low velocity and a limited motion. It can be connected to the solid fraction of the granular gas.

4.3 Solid fraction

We compute the local solid fraction $\phi(L_p,z)$ occupied by the spheres, in a similar fashion to what is usually performed in close packing and jamming transitions [28,29]. In the latter, the system develops yield stress in a disordered state which is achieved numerically by introducing sphere interactions which mimic contact forces [30] out of which the pressure tensor can be computed [28]. Here, as the contacts are supposed to be instantaneous, such an approach is of course irrelevant. Figure 8 shows the solid fraction as a function of the altitude and the longitudinal coordinate L_p for the angle $\alpha = 40°$, and highlights the increased stacking which occurs at the top of the chamber. We find that $\phi(L_p, z) > 0.20$ close to the acute angle. Large variations are found in the box, $\phi(L_p, z)$ being about 1×10^{-3} in the major part, but displaying also a slight increase close to the top wall. One should finally note that the maximum value of $\phi(L_p, z)$ obtained is still very low (0.26) compared to usual threshold values ϕ_c obtained in the context of jamming transitions, which range from 0.58 for diluted to 0.63 for more dense systems [28].

Here one can remark the very dense regions close to the top angle of the prism, and also along the side wall on the right; these regions have a density difference of about a factor

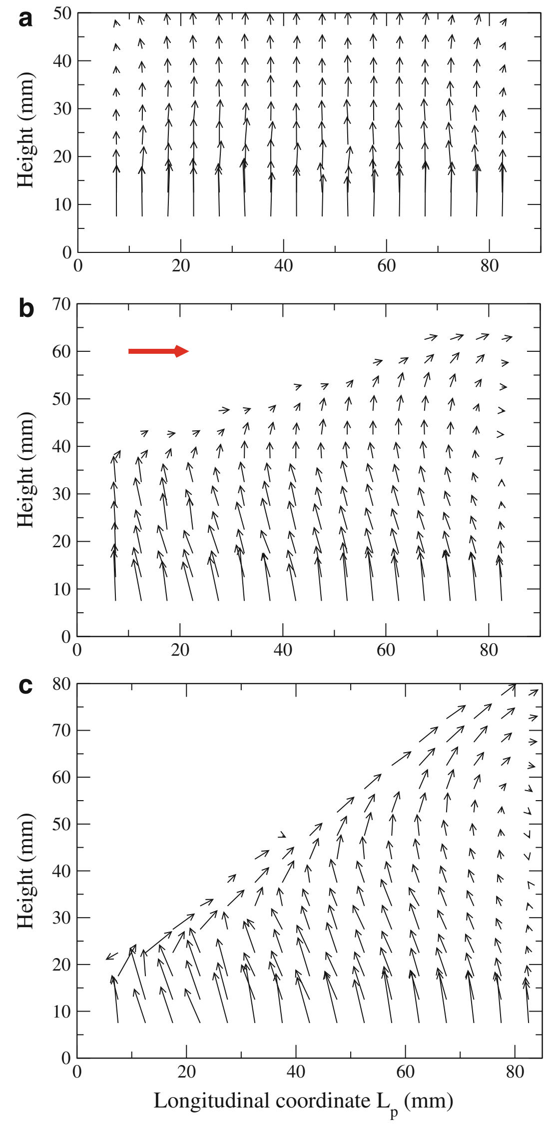

Fig. 7 (Color online) Velocity field within the granular gas in the prism geometry for three different angles: **a** $\alpha = 0°$, **b** $\alpha = 20°$, and **c** $\alpha = 40°$. The *horizontal red arrow* represents 2.0 m/s

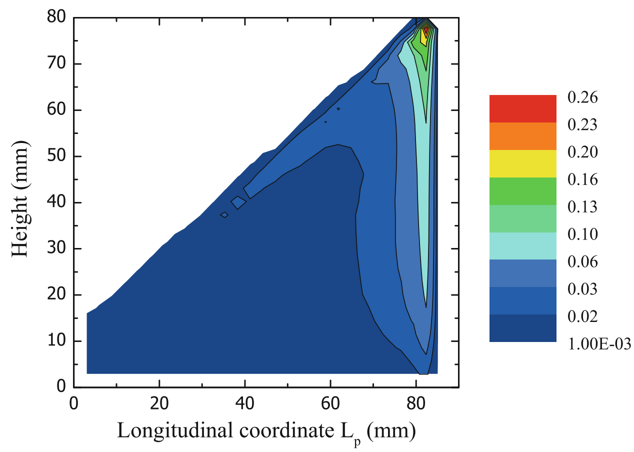

Fig. 8 (Color online) Contourplot (L_p,z) of the solid fraction $\phi(L_p, z)$ for $\alpha = 40°$

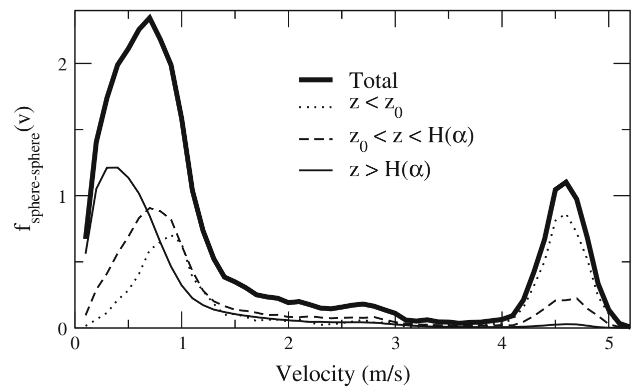

Fig. 9 Sphere-sphere impact velocity distribution in the trapezoidal box with $\alpha = 40°$ splitted into three regions: $z<z_0$ (*dotted line*), $z_0 < z < H(\alpha)$ (*broken line*) and $z > H(\alpha)$ (*solid line*). Here $z_0 = 1.5\sigma$

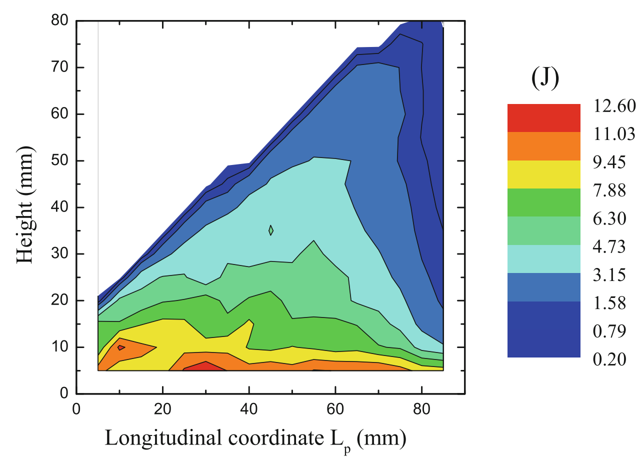

Fig. 10 (Color online) Contourplot of the granular temperature (in J) for $\alpha = 40°$

10 with respect to the less denser regions (low altitude and $L_p \simeq 0$).

The sphere-sphere impacts can be further analyzed by considering the corresponding impact velocity between spheres $f_{sphere-sphere}(v)$ (Fig. 9). Here, we split the distribution into contributions depending on the location of the impact: $z < z_0$, $z_0 < z < H(\alpha)$ and $z > H(\alpha)$, and z_0 is chosen to be close to the vibrating bottom wall ($z_0 \simeq 1.5\sigma = 5$ mm) so that we can discriminate impacts occuring either in the vicinity of the sonotrode, or in the lower part of the chamber, or in the region of the top wall and top angle. It can be clearly stated that the peak found at low velocity arises from all regions with identified contributions in the main peak at 0.5 m/s, i.e. one has velocity contributions at 0.4, 0.8 and 0.9 m/s for $z < z_0$, $z_0 < z < H(\alpha)$ and $z > H(\alpha)$, respectively. Moreover, by analyzing in the same fashion the peak found at high velocity (4–5 m/s), it becomes clear that it is a property of the granular gas close to the sonotrode. The peak is indeed nearly absent when the upper region of the chamber is considered, and is mostly obtained from the region $z < z_0$.

From Fig. 8, one furthermore notes that a large number of collisions takes place in the immediate vicinity of the top surface where the solid fraction $\Phi(L_p,z)$ is increased and where the velocity is low. Here, spheres act as obstacles for the other spheres moving upwards with a higher velocity (Fig. 7b, c). These will eventually avoid the higher density region of weakly moving spheres (i.e. quasi immobile, Fig. 8), and will arrive on the top surface with a tangential direction. This will contribute to nearly tangential impacts near the top wall with impact velocity growing as α is increased. The number of impact angles of 90° thus grows substantially. Similarly, the maximum in the IFUS obtained at around 10 mm (Figs. 2c, 3b) can be understood from the velocity field profile inside the box. Particles evolve from a quasi-vertical motion when $\alpha = 0°$ to trajectories that are nearly perpendicular to the normal surface vector $\mathbf{n_t}$ when the top surface is tilted ($\alpha \neq 0$). If one splits the IFUS of Fig. 3 into a contribution having an impact angle α_i larger than e.g. 80°, one remarks that the maximum found is indeed originated by such tangential impacts.

4.4 Granular temperature

Figure 10 shows the granular temperature as a function of the altitude and the longitudinal coordinate L_p for the angle $\alpha = 40°$. One recovers part of the observations and results obtained previously. Hot particles are found close to the vibrating bottom wall. At the altitude $H(\alpha)$, the temperature has dropped by a factor of 2, although the number of possible sphere-sphere collisions is small. But one has to remember that spheres being accelerated by the bottom wall (sonotrode) have a high velocity, which involves a low restitution coefficient at each sphere-sphere collision (e.g. of about 0.6 for velocities of about 5 m/s [12]). As a consequence, the velocity (temperature) loss at each collision with other spheres is important so that after a few collisions close to the sonotrode, the granular temperature has substantially decreased.

A cold region made of weakly moving spheres is found in the vicinity of the top angle, and also close to the wall containing the acute angle ($\pi/2 - \alpha$). The global shape of the cold regions appears to correlate with the one obtained from sphere-sphere collisions (regions with a high solid fraction, see Fig. 8) for which the velocity is found to be very small ($0.20 < \mathrm{T} < 3.15$). The nearly immobile region found along the wall containing the acute angle (seen in Fig. 10, and also from Fig. 7c) has a surprising shape, with a spatial extension up to one third of the chamber at half of the total altitude. It is the result of the combined phenomena that we have described above: sphere adorption on the side wall and confinement, which traps spheres at the top of the box through enhanced sphere-sphere and sphere-wall collisions. In addition, the high velocity stream of spheres being accelerated at zero altitude maintains these nearly immobile regions (Fig. 7c).

In contrast with findings from granular kinetic theory [31] and experimental results for vibrofluidized granular beds [32], one does not obtain a minimum for the granular temperature with the box height. Once the conservation laws (continuity and momentum) and the constitutive relations being established, most of the properties and the granular gas depend on the boundary conditions of the system. Usually, such sets of kinetic theory equations are simplified by the absence of a top wall which ensures that in the limit $z \to \infty$ collisions become infrequent [31,33]. We keep this issue for further investigation, and clearly the study of a combined effect on the kinetic theory equations (additional boundary condition on the top, and strong density gradient induced by the acute angle) is beyond the scope of this contribution.

5 Conclusions

We have shown that the effect of the chamber geometry in a vibrated granular gas could modify substantially not only its properties but also the spheres impact on the chamber walls, and especially the top wall. While the effect of inelastic collisions in granular media are well known and documented, little is known on how spatial limitation modifies the local properties of a granular gas. Here, we have shown from simple geometries how the properties of a granular gas are modified in this context. The combination of inelastic collisions and spatial limitation leads to surprising properties that can be tuned continuously in the case of a simple box with prismatic geometry. Velocity, angle and surface impact distributions are shown to be highly sensitive to such geometries, and it appears that in regions where the space for motion is limited with a dimension of the order of magnitude of the sphere size, sphere-wall collisions are enhanced and bring the gas to a local densified state. Density is increased by a factor of about 5 with respect to the nominal one η. In the present prism geometry, such situation is met in the vicinity of the acute angle of the prism where stacking takes place. As a result, the whole dynamics (velocity, impact angles, granular temperature) of the gas is modified and becomes strongly heterogeneous.

While these effects are moderate here, given the chosen gas density of $\eta = 1.3 \times 10^{-3}\,\mathrm{mm}^{-3}$, we anticipate that increased densitites in the presence of spatial limitations/confinement should lead to even more surprising phenomena as stacking and side wall collisions should be even more enhanced.

Finally, the present study is certainly timely for the improvement of potential applications. In fact, ultrasonic shot peening processes have shown that the treated materials have a lower roughness and a better surface quality when compared to materials treated only by conventional air projected shot peening. As this has some direct influence on fatigue-life enhancement and on the presence of residual stresses at and just below the treated surface, an improved understanding on how the control parameters will affect the impact dynamics is needed. Here we have shown that both the impact velocity and impact angle can be substantially affected by the geometry of the peeing chamber. Results show an increased heterogeneous treatment when the top surface is tilted with respect to the vibrating sonotrode at the bottom.

Acknowledgments It is a pleasure to acknowledge ongoing discussions and support from D. Le Saunier, V. Desfontaine, G. Doubre, S. Mechkov, M. Prioul, P. Renaud, J. Talbot and P. Viot. SNECMA (Groupe Safran) and SONATS (Europe technologies Group) are gratefully acknowledged for financial support.

References

1. Goldhirsch, I.: Rapid granular flows. Annu. Rev. Fluid Mech. **35**, 267–293 (2003)
2. de Gennes, P.-G.: Granular matter : A tentative view. Rev. Mod. Phys. **71**, S374–S382 (1999)
3. Capriz, G., Giovine, P. (eds.): Mathematical Models of Granular Matter. Springer, Berlin (2008)
4. Brillantov, N.V., Pöschel, T.: Kinetic Theory of Granular Gases. Oxford University Press, Oxford (2004)
5. Nicodemi, M.: Dynamical response functions in models of vibrated granular media. Phys. Rev. Lett. **82**, 3734–3737 (1999)
6. Nicodemi, M., Coniglio, A.: Aging in out of equilibrium dynamics of models for granular media. Phys. Rev. Lett. **82**, 916–919 (1999)
7. Talbot, J., Viot, P.: Wall-enhanced convection in vibrofluidized granular systems. Phys. Rev. Lett. **89**, 064301 (2002)
8. Johnson, O., Toussaint, R., Maloy, K.J., Flekkoy, E.G.: Pattern formation during air injection into granular materials confined in a circular Hele-Shaw cell. Phys. Rev. E **74**(1–13), 011301 (2006)
9. Kudrolli, A.: Size separation in vibrated granular matter. Rep. Prog. Phys. **67**, 209–247 (2004)

10. Ferreira, J.A.M., Boorrego, L.F.P., Costa, J.D.M.: Effects of surface treatments on the fatigue of notched bend specimens. Fatigue Fract. Eng. Mater. Struct. **19**, 111–117 (1996)
11. Zum Gahr, K.-H.: Microstructure and Wear of Materials. Tribology Series. Elsevier, Amsterdam (1987)
12. Micoulaut, M., Retraint, D., Viot, P., François, M.: Heterogeneousutrasonic shot peening: Experiment and simulation. In: Proceedings of the International Conference on Shot Peening, 9, 119-125 (2005)
13. Micoulaut, M., Mechkov, S., Retraint, D., François, M., Viot, P.: Granular gases in mechanical engineering: On the origin of heterogeneous ultrasonic shot peening. Granul. Matter **9**, 25–33 (2007)
14. Lu, J., Peyre, P., Nonga, C.O., Benamar, A., Flavenot, J.F.: Residual Stress and Mechanical Surface Treatments. SEM, Baltimore (1994)
15. Badreddine, J., Rouhaud, E., Micoulaut, M., Retraint, D., Remy, S., François, M., Baboeuf, G., Desfontaine, V.: Simulation and experimental approach for shot velocity evaluation in ultrasonic shot peening. Mécanique et Industrie **12**, 223–229 (2011)
16. Wang, K., Tao, N.R., Liu, G., Lu, J., Lu, K.: Plastic strain-induced grain refinement at the nanometer scale in copper. Acta Materialia **54**, 5281–5291 (2006)
17. Goldsmith, W.: The Theory and Physical Behaviour of Colliding Solids. Dover Ed, London (1990)
18. Hertzsch, J.M., Spahn, F., Brilliantov, N.V.: On low-velocity collisions of viscoelastoc particles. J. Phys. II **5**, 1725–1735 (1995)
19. Brilliantov, N.V., Spahn, F., Hertzsch, J.M., Pöschel, T.: Models for collisions in granular gases. Phys. Rev. E **53**, 5382–5392 (1996)
20. Schwager, T., Pöschel, T.: Coefficient of normal restitution of viscous particles and cooling rate of granular gases. Phys. Rev. E **57**, 650–654 (1998)
21. Johnson, K.L.: Contact Mechanics. Cambridge University Press, Cambridge (1985)
22. Zener, C.: The intrinsic inelasticity of large plates. Phys. Rev. **59**, 669–673 (1941)
23. Sondergaard, R., Chaney, K., Brennen, C.E.: Measurements of solid spheres bouncing off flat plates. J. Appl. Mech. **57**, 694 (1990)
24. Micoulaut, M., Retraint, D., Viot, P., Francois, M.: Grenaillage ultrasonore hétérogène. Actes du 17ème Congrès Français de Mécanique **689**, 1–6 (2005)
25. McNamara, S., Falcon, E.: Simulation of vibrated granular medium with impact-velocity-dependent restitution coefficient. Phys. Rev. E **71**, 031302 (2005)
26. Brach, R.M.: Impact dynamics with applications to solid particle erosion. Int. J. Impact Eng. **7**, 37–53 (1988)
27. Talbot, J., Viot, P.: Torroidal convection roll in a three-dimensional granular system. Physica A **317**, 672–676 (2002)
28. O'Hern, C.S., Silbert, L.E., Liu, A.J., Nagel, S.R.: Jamming at zero temperature and zero applied stress: The epitome of disorder. Phys. Rev. E **68**, 011306 (2003)
29. Torquato, S., Truskett, T.M., Debenedetti, P.M.: Is random close packing of spheres well defined. Phys. Rev. Lett. **84**, 2064–2067 (2000)
30. Berthier, L., Jacquin, H., Zamponi, F.: Microscopic theory of the jamming transition of harmonic spheres. Phys. Rev. E **84**, 051103 (2011)
31. Viswanathan, H., Wildman, R.D., Huntley, J.M., Martin, T.W.: Comparison of kinetic theory predictions with experimental results for a vibrated three-dimensional granular bed. Phys. Fluids **18**, 113302 (2006)
32. Wildman, R.D., Huntley, J.M., Parker, D.J.: Granular temperature profiles in three-dimensional vibrofluidized granular beds. Phys. Rev. E **63**, 061311 (2001)
33. Javier Brey, J., Ruiz-Montero, M.J., Moreno, F.: Hydrodynamics of an open vibrated granular system. Phys. Rev. E **63**, 061305 (2001)